宇宙线加速的非弹性暗物质的直接探测

康现伟

xwkang@bnu.edu.cn

北京师范大学

第二届地下和空间粒子物理与宇宙物理前沿问题研讨会，千岛湖，2023年5月7-12日

JHEP

PUBLISHED FOR SISSA BY SPRINGER

RECEIVED: *October 27, 2021*
REVISED: *February 22, 2022*
ACCEPTED: *March 25, 2022*
PUBLISHED: *April 14, 2022*

Revising inelastic dark matter direct detection by including the cosmic ray acceleration

Jie-Cheng Feng,[a] Xian-Wei Kang,[b,c,1] Chih-Ting Lu,[d] Yue-Lin Sming Tsai[e,1] and Feng-Shou Zhang[b,c]

特别鸣谢

冯杰成，北师大2018级本科生，现在苏黎世联邦理工读硕

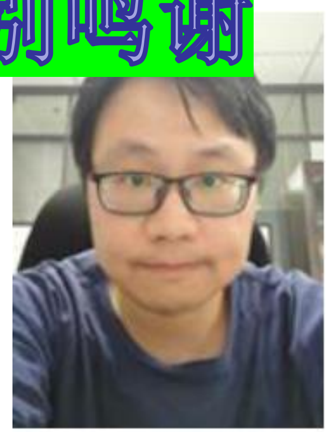

蔡岳霖，中科院紫金山天文台

卢致廷，南京师范大学

目录

- 引言
- 非弹性暗物质的有效相互作用
- vDM和CRDM的探测
- 目前测量对参数的限制(PandaX-4T为例)
- 结论和展望

名词解释

- **DM:** dark matter
- **vDM:** virialized DM，低速
- **CDRM:** cosmic ray accelerated vDM
- **DD:** direct detection

引言

1. 非引力证据缺失，与标准模型粒子如何相互作用

2. XENON1T和PandaX-4T的测量已将DM-proton弹性散射截面推到中微子地板 [XENON, PRL 121 (2018) 111302; PandaX-4T, PRL127 (2021) 261802]

3. 非相对论vDM对探测阈的限制，如质量为5 GeV以下的暗物质成为xenon型探测器的盲区

4. 若要探测质量劈裂为100 keV量级的暗物质χ_1和χ_2，传统vDM质量需要重到TeV量级[PandaX-II, PRD 96 (2017) 102007]

Inelastic dark matter (hep-ph/0101138) was originally proposed to explain DAMA not through a change in couplings, but rather through a change in kinematics.

cosmic ray accelerated vDM (CRDM)

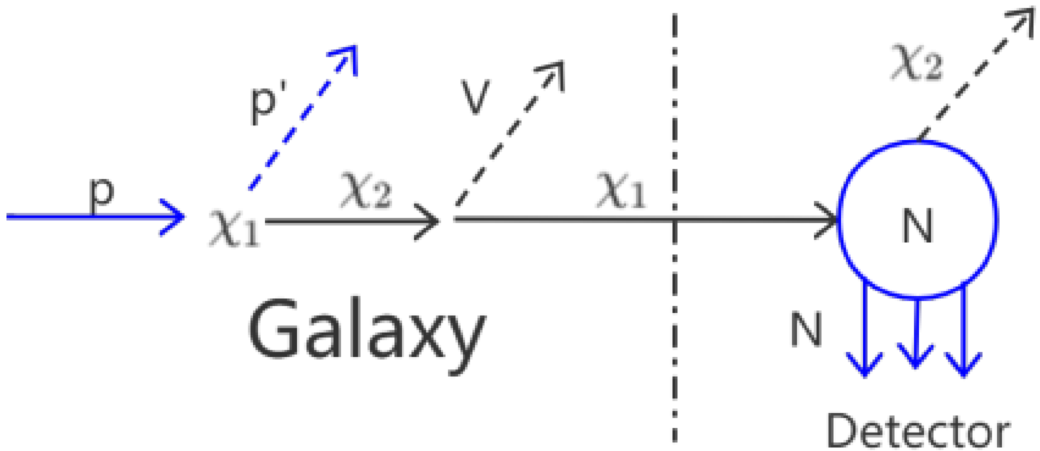

Cosmic ray accelerated inelastic DM detection scenario: $p + \chi_1 \to p' + \chi_2 \to p' + \chi_1 + V$. By this mechanism, the final χ_1 is accelerated

p denotes the CR proton or helium

the prime is used to distinguish the same particles in the initial and final states

the inelastic DM χ_1 and χ_2 are the ground state and excited state, respectively

V is the mediator between SM and DM

N is the target nucleus inside the underground detector

非弹性暗物质的有效相互作用

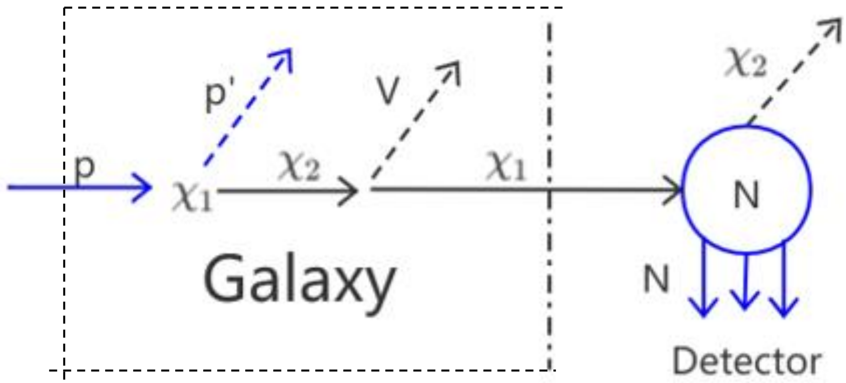

The common nucleon-V interactions are

$$\mathcal{L}_{VN} = \overline{N}\gamma^{\mu}\left(C_N^v + C_N^a\gamma^5\right) N V_{\mu}.$$

The completed Lagrangian to describe $p + \chi_1 \to p' + \chi_2$ process is $\mathcal{L}_{VN} + \mathcal{L}_{VD}$

We consider both fermionic DM interaction and scalar dark matter interaction for $\mathcal{L}_{VD}$

$$\mathcal{L}_1^f = \left[\overline{\chi_2}\gamma_\mu \left(C_\chi^v + C_\chi^a \gamma^5\right)\chi_1 + h.c.\right] V^\mu,$$

$$\mathcal{L}_2^f = \frac{1}{\Lambda_{E(M)}}\bar{\chi}_2 \sigma_{\mu\nu}\Gamma_{E(M)}\chi_1 F_V^{\mu\nu},$$

$$\mathcal{L}_1^s = g_\chi(\chi_1 \partial^\mu \chi_2 - \chi_2 \partial^\mu \chi_1)V_\mu,$$

$$\mathcal{L}_2^s = \frac{1}{\Lambda_s^2}(\partial_\mu \chi_2 \partial_\nu \chi_1)F_V^{\mu\nu}.$$

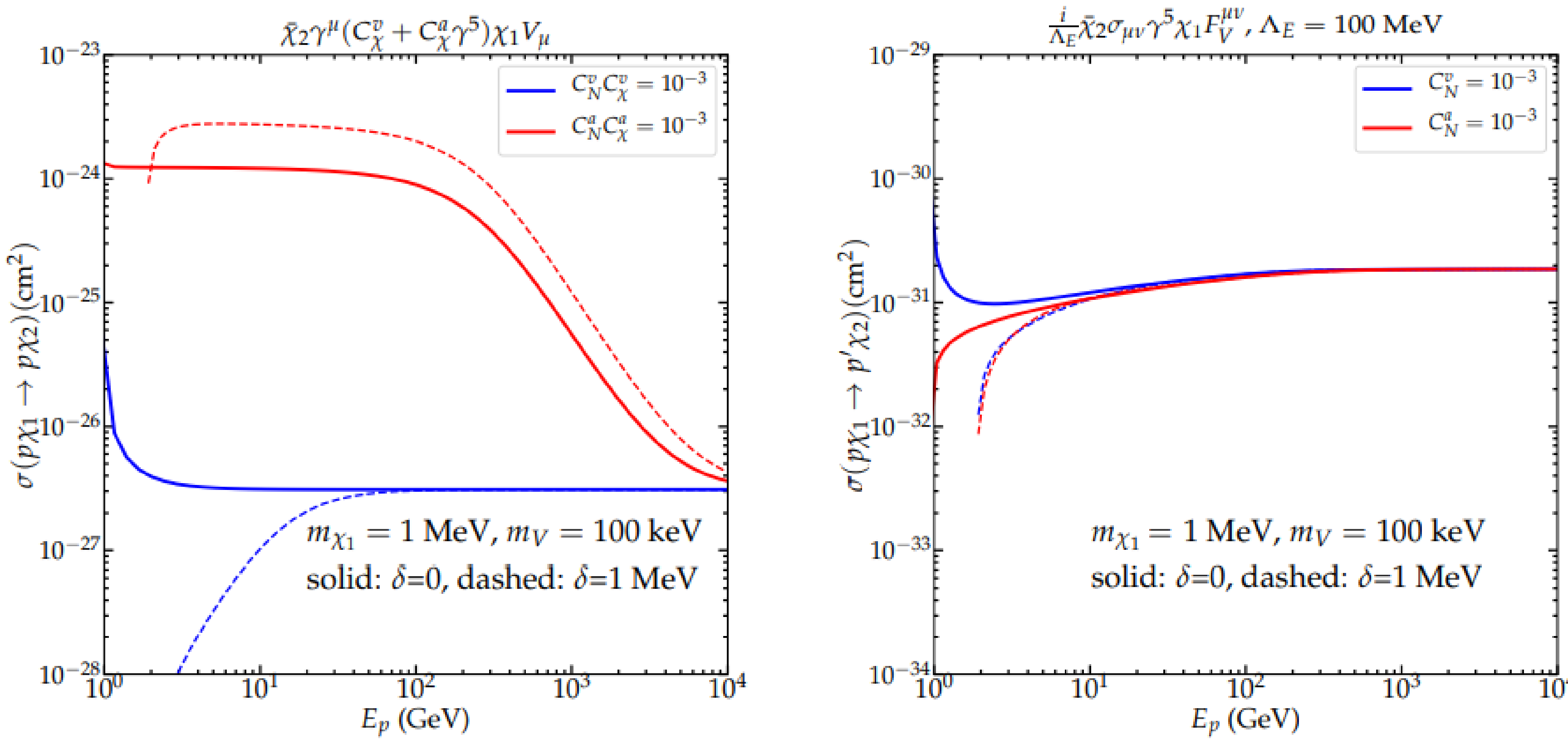

(a) $\mathcal{L}^f_1$.

(b) $\mathcal{L}^f_2$

The integrated cross section of process $p\chi_1 \to p'\chi_2$ as a function of incoming proton energy E_p

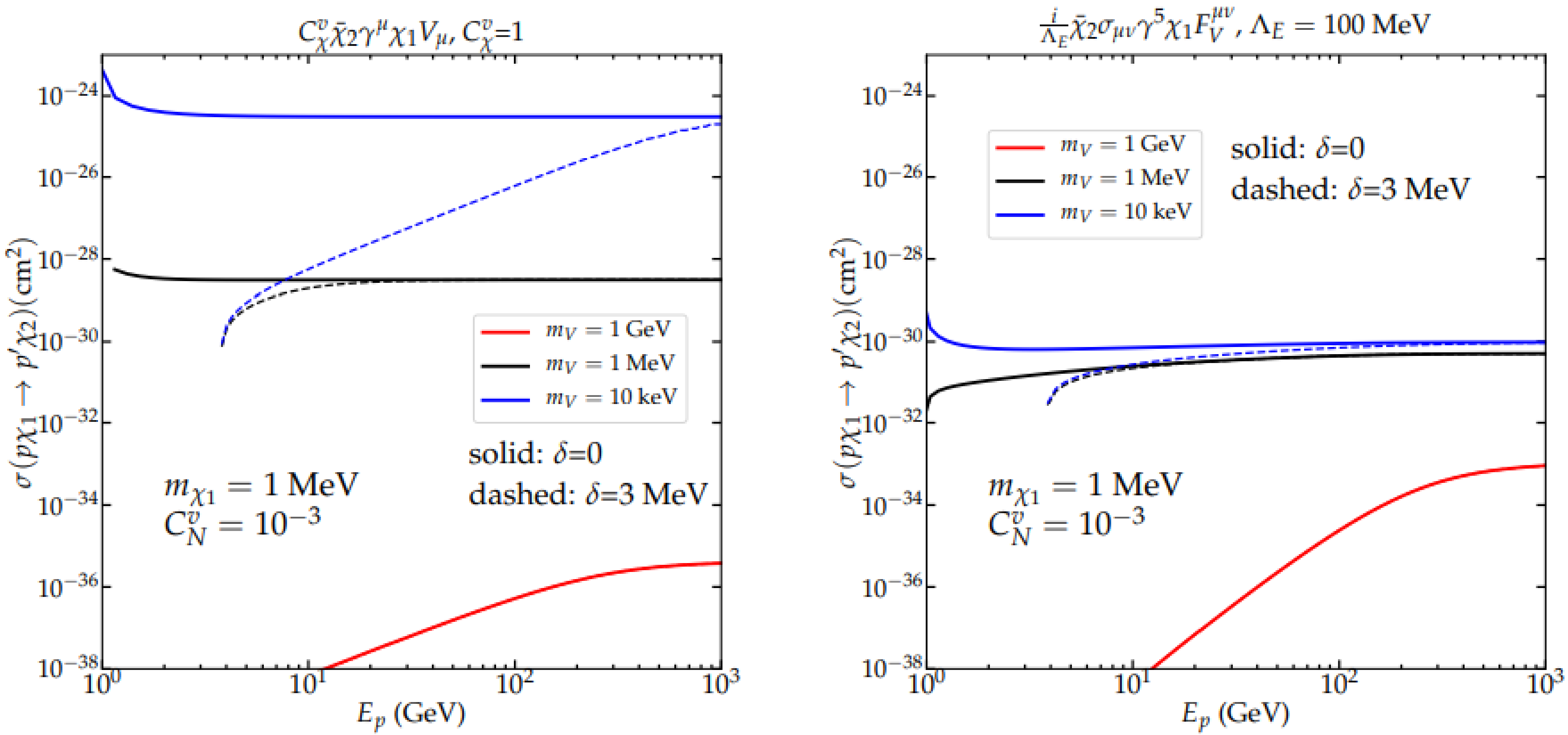

(a) $\mathcal{L}_1^f$ (b) $\mathcal{L}_2^f$

The integrated cross section of process $p\chi_1 \to p'\chi_2$ as a function of incoming proton energy E_p

vDM和CRDM探测

Traditional detection of the virialized DM

For a mass splitting δ between χ_1 and χ_2, a minimum velocity

$$v_{\min}(Q) = \frac{1}{\sqrt{2m_{\mathcal{T}}Q}}\left(\frac{m_{\mathcal{T}}Q}{\mu_{\chi N}} + \delta\right),$$

with Q energy recoil, $m_{\mathcal{T}}$ target mass, μ reduced mass

The differential event rate of scattering between DM and the target nucleus per unit detector mass with respect to the recoil energy Q:

$$\frac{\mathrm{d}\mathcal{R}}{\mathrm{d}Q} = \sum_{\mathcal{T}} \frac{\xi_{\mathcal{T}}}{m_{\mathcal{T}}} \int_{T_\chi[v_{\min}(Q)]} \boxed{\frac{d\phi_\chi}{dT_\chi}} \frac{\mathrm{d}\sigma_{\chi\mathcal{T}}}{\mathrm{d}Q}\, dT_\chi.$$

DM flux

The total event rate $\mathcal{R} = \int_0^\infty \boxed{\epsilon(Q)} \frac{\mathrm{d}\mathcal{R}}{\mathrm{d}Q} dQ.$

efficiency

Spin independent part

$$\frac{\mathrm{d}\sigma^{\mathrm{SI}}_{\chi\mathcal{T}}}{\mathrm{d}Q} = \frac{\mathrm{d}\sigma^{\mathrm{SI}}_{\chi p}}{\mathrm{d}Q} \times \frac{\mu^2_{\mathcal{A}}}{\mu^2_p} \times \left[\mathcal{Z} + \frac{f_n}{f_p}(\mathcal{A} - \mathcal{Z})\right]^2 \times \underline{F^2(Q, \mathcal{A}, \mathcal{Z})}$$

Helm type form factor

$$\frac{d\phi_{\chi_1}^{\rm MW}}{dT_{\chi_1}} = \frac{\rho_0}{m_{\chi_1}} \times D_{\rm eff} \times \sum_{i=p,{\rm He}} \int dE_i \frac{d\phi_i}{dE_i} G_i^2(2m_{\chi_1}T_{\chi_1}) \frac{d\sigma_{p\chi_1 \to p'\chi_1 V}}{dT_{\chi_1}}$$

The $G_i^2(Q^2)$ here is simply taken in its dipole form:

$$G_i^2(Q^2) = \left[1 + \frac{Q^2}{\Lambda_i^2}\right]^{-4}$$

Λ_p= 770 MeV
Λ_{He} = 410 MeV.

Considering that the form factor relates $\sigma_{\chi p}$ to $\sigma_{\chi\mathcal{T}}$, the inelastic cross section of DM-target scattering is:

$$\frac{d\sigma_{\chi\mathcal{T}}}{dQ}(m_{\chi_1}, \delta, m_V, Q) = \left.\frac{d\sigma_{\chi\mathcal{T}}}{dQ}\right|_{\rm EFT} \times \frac{\mathcal{M}_{\chi p}^2(m_{\chi_1}, \delta, m_V, Q)}{\mathcal{M}_{\chi p, {\rm EFT}}^2} \qquad (22)$$

where the effective operator cross section $\frac{d\sigma_{\chi\mathcal{T}}}{dQ}|_{\rm EFT}$ is obtained with the publicly available numerical code LikeDM-DD [33]. $\mathcal{M}_{\chi p}^2(m_{\chi_1}, \delta, m_V)$ are calculated in Appendix B, but $\mathcal{M}_{\chi p, {\rm EFT}}^2$ is used with $\delta = 0$ and the limit $m_V \gg Q$.

$$\boxed{\frac{d\mathcal{R}}{dQ} = \sum_{\mathcal{T}} \frac{\xi_{\mathcal{T}}}{m_{\mathcal{T}}} \int_{T_{\tt min}}^{\infty} dT_{\chi_1} \frac{d\sigma_{\chi_1\mathcal{T}}}{dQ} \frac{d\Phi_{\chi_1}^{\rm MW}}{dT_{\chi_1}},}$$

DRU or keV^{-1} kg^{-1}day^{-1}

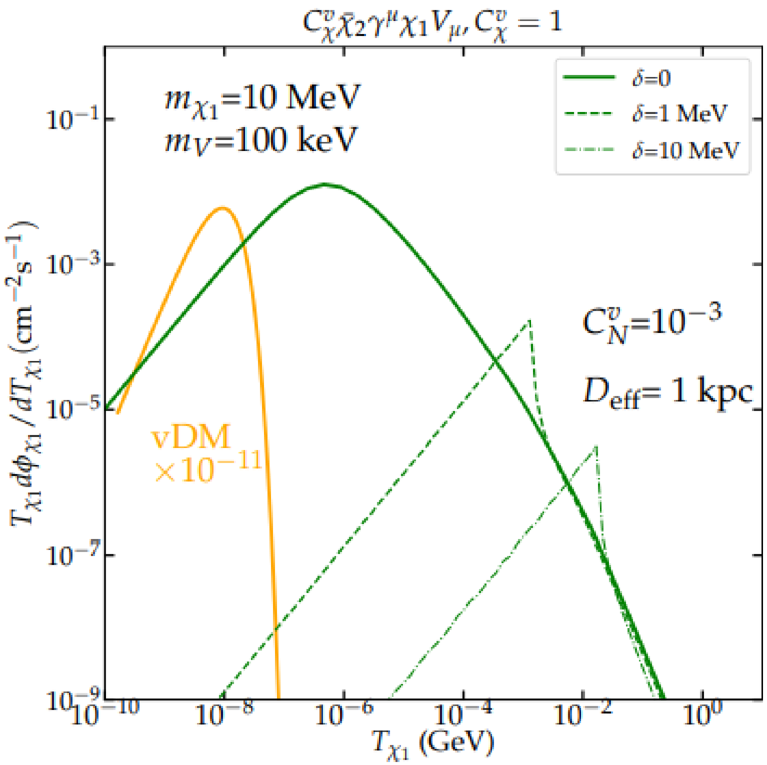

(a) CRDM versus vDM .

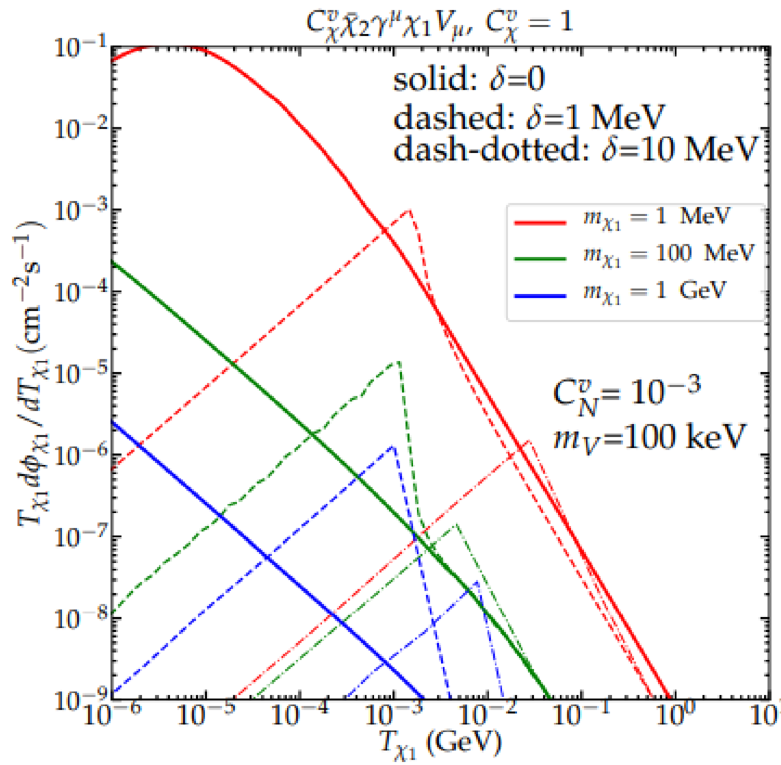

(b) CRDM fluxes.

FIG. 6. (a) Comparison of vDM and CRDM fluxes. Both vDM and CRDM fluxes are obtained by using $\bar{\chi_2}\gamma^\mu\chi_1V_\mu$ interaction with $m_{\chi_1}=10\,\text{MeV}$, $m_V=100\,\text{keV}$, and $C^a_N=10^{-3}$. The value of $D_{\rm eff}$ for CRDM is fixed to 1 kpc as a default value. (b) Spectra of CRDM with the VV interaction. Three benchmarks of DM mass 1 MeV (red lines), 100 MeV (green lines), and 1 GeV (red lines) are presented. We also plot three different mass splittings, $\delta=0$ (solid lines), $\delta=1\,\text{MeV}$ (dashed lines), and $\delta=10\,\text{MeV}$ (dash-dotted lines).

特点: (1) those non-degenerated curves show sharp peaks at $T_{\rm sp}$

- the CRDM energy spectrum is the product of the distribution $d\sigma_{p\chi_1}/dT_{\chi_1}$ and CR energy spectrum.
- the cross section is flat at high energy, but the δ contribution dominates $d\sigma_{p\chi_1}/dT_{\chi_1}$ in the lower energy region.
- Thus in the small energy region $T_{\chi_1} < T_{\rm sp}$, the spectrum is strongly affected by $d\sigma_{p\chi_1}/dT_{\chi_1}$

(2) δ can cause a sharp peak $T_{\rm sp}$ in the spectrum toward higher energy but with a decline of total flux.

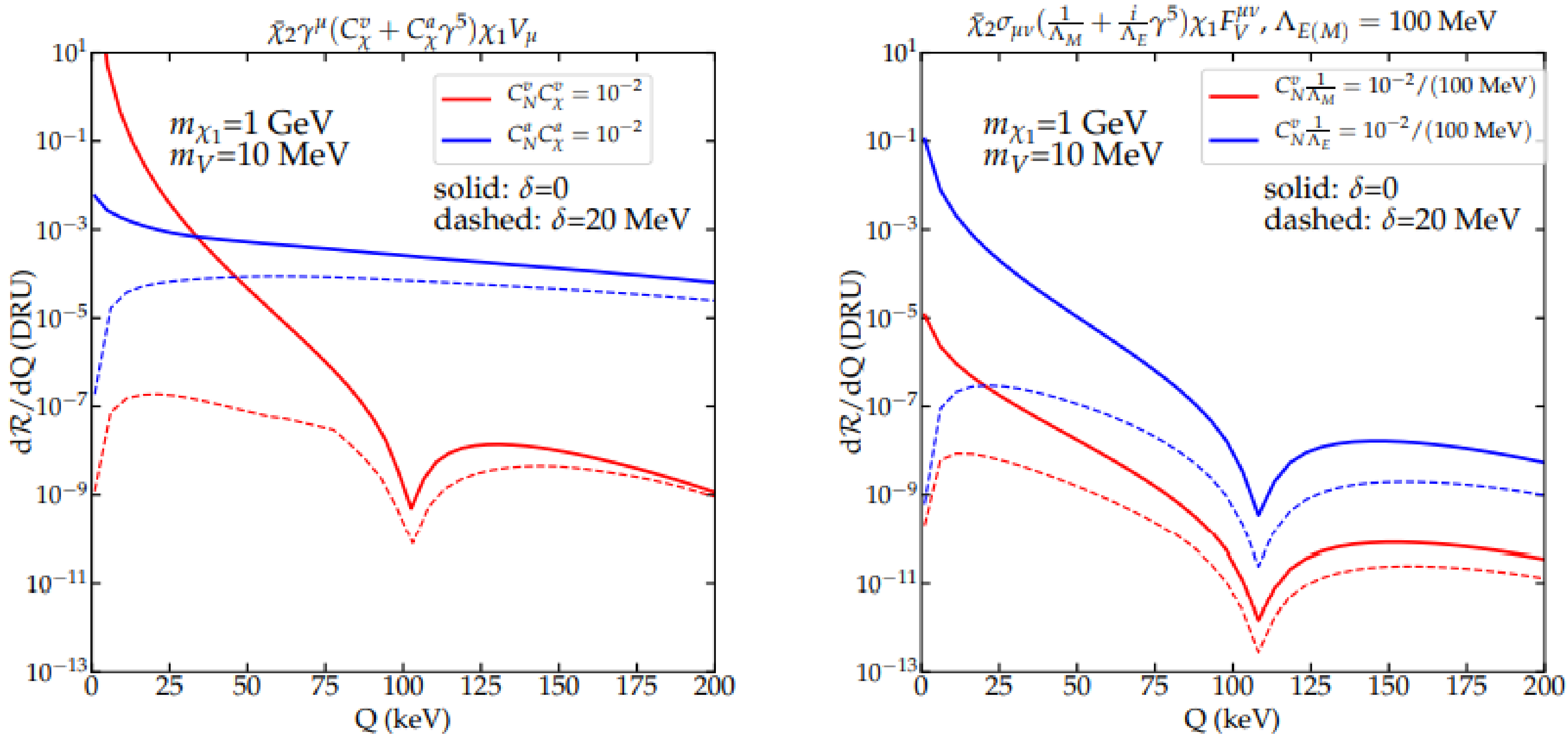

(a) VV and AA interactions.

(b) ED and MD interactions.

FIG. 8. Detection rate $d\mathcal{R}/dQ$ (DRU or $\mathrm{keV}^{-1}\mathrm{kg}^{-1}\mathrm{day}^{-1}$) of fermionic CRDM $\chi-$xenon scattering for $\mathcal{L}^f_1$ (left) and $\mathcal{L}^f_2$ (right). The mass degenerated cases $\delta = 0$ are represented as solid lines, while the dashed lines are for $\delta = 20\,\mathrm{MeV}$.

we use $\mathcal{R} \sim$ 4/0.63/tonne/year projected onto the (δ, C_N) and (m_{χ_1}, δ) planes to show the detection capability of PandaX-4T.

1. AA interaction can give the most stringent limit on C_N while the higher dimensional operators, especially MD, have weaker limit

2. A turning point then appears in all the interactions, and the limits behave differently at the smaller and larger m_{χ_1} regions.

3. PandaX-4T provides the most stringent 21 limit for AA in the large m_{χ_1} region but for VV in the lower m_{χ_1} region.

4. With the help of the CRDM scenario, the PandaX-4T exclusion of δ can be extended to 0.1 GeV, even 1 GeV in some cases

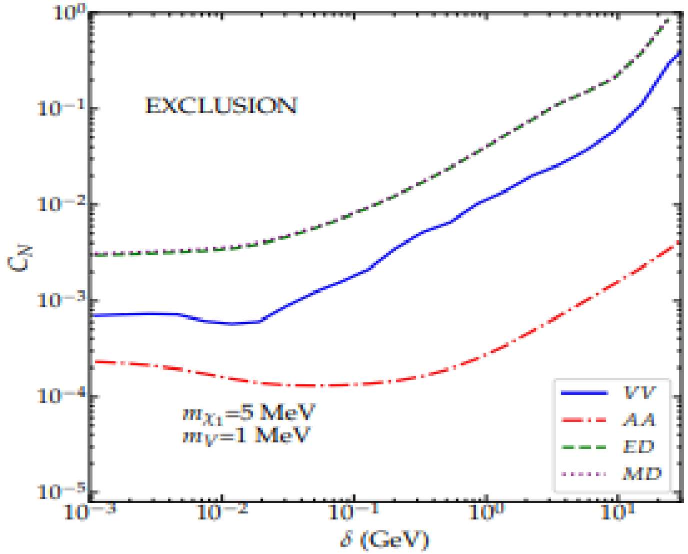

(a) $m_{\chi_1} = 5\,\mathrm{MeV}$.

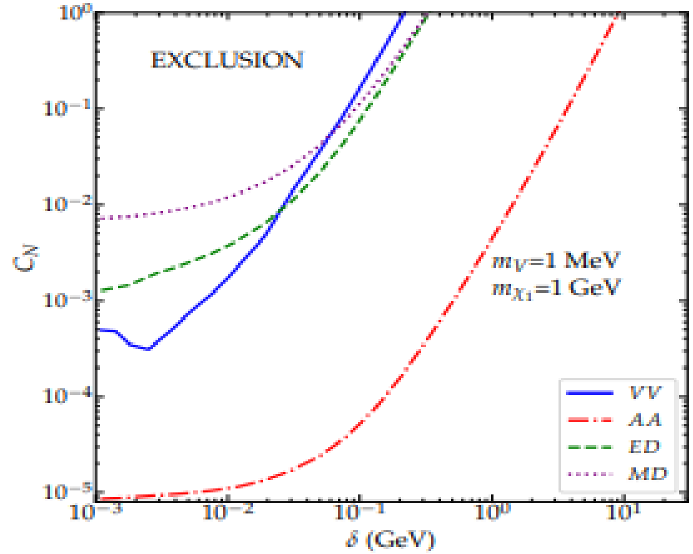

(b) $m_{\chi_1} = 1\,\mathrm{GeV}$.

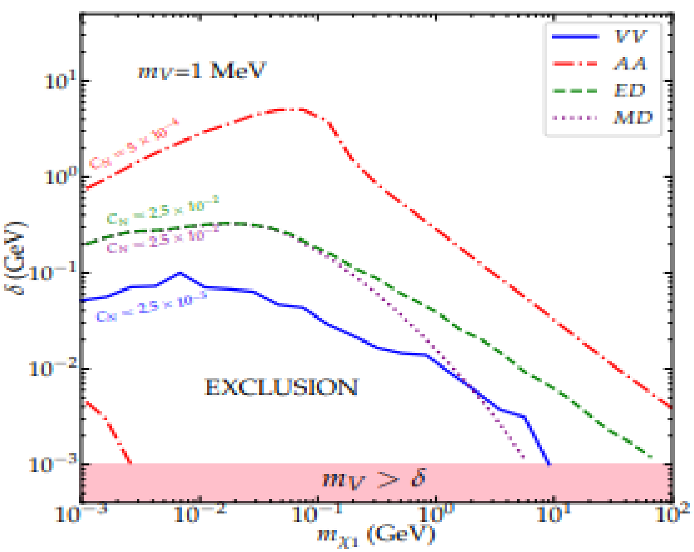

(c) $m_V = 1\,\mathrm{MeV}$.

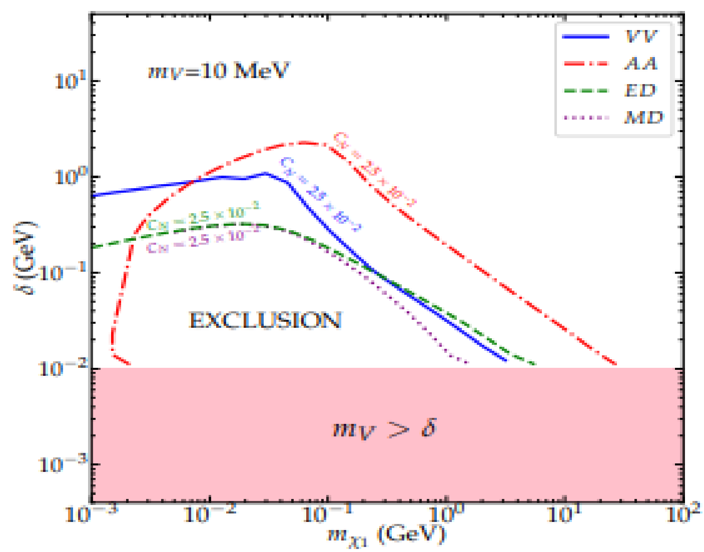

(d) $m_V = 10\,\mathrm{MeV}$.

Because of the higher kinetic energy of CRDM, the PandaX-4T data ***can probe sub-GeV DM region in CRDM but not in vDM scheme.***

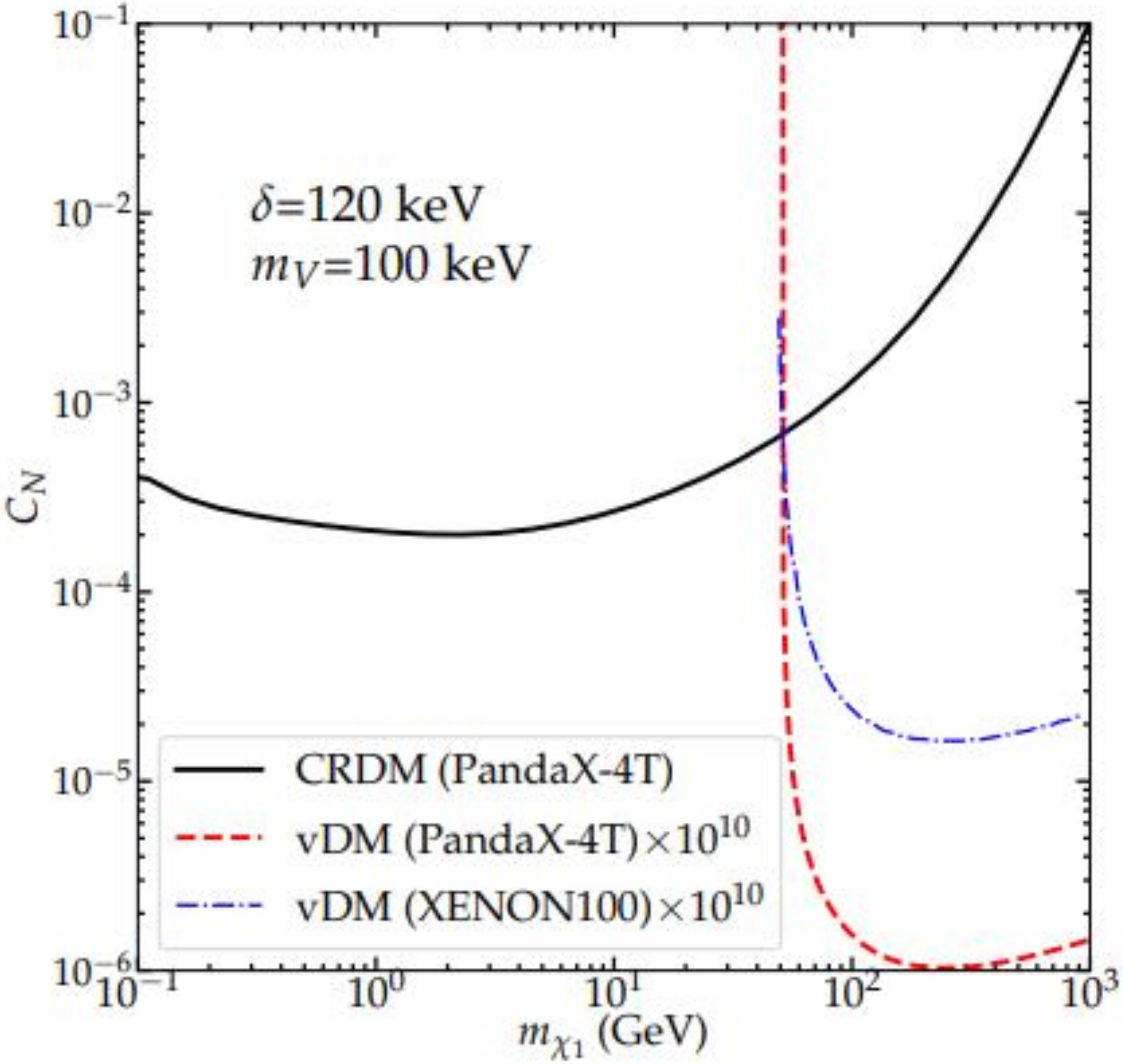

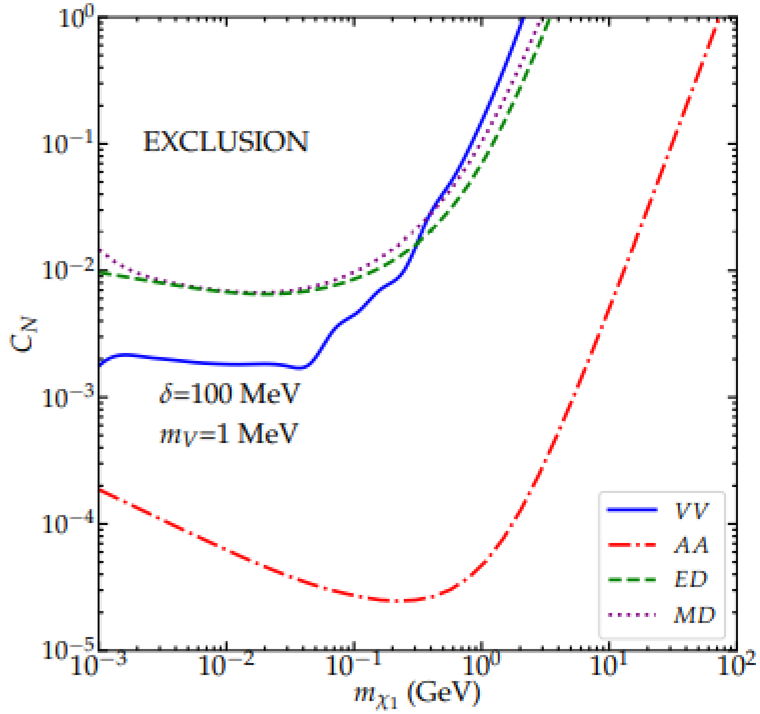

(a) $\delta = 100\,\mathrm{MeV}$

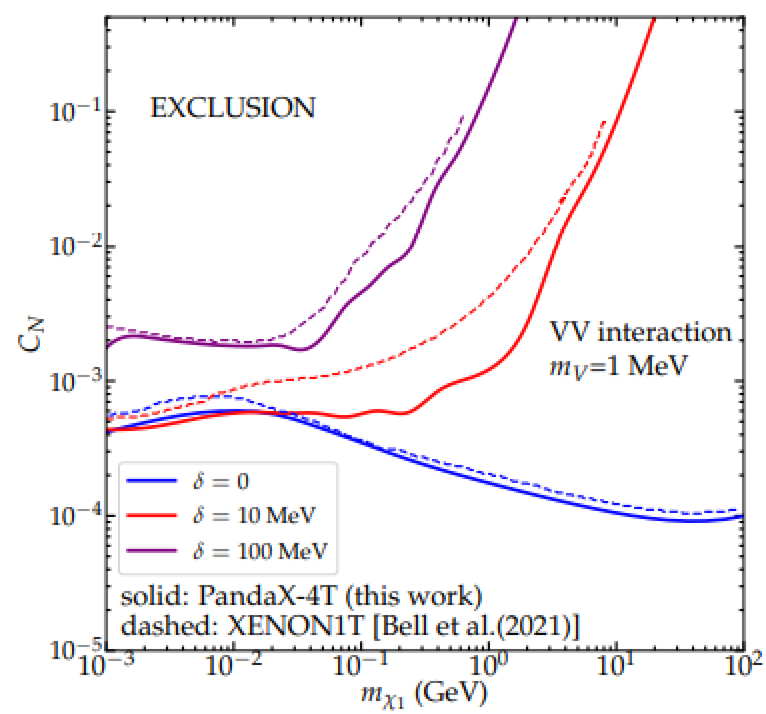

(b) VV

FIG. 10. 95% upper limits projected in the (m_χ, C_N) plane. (a) the limits with fixed values $\delta = 100\,\mathrm{MeV}$ and $m_V = 1\,\mathrm{MeV}$ for VV, AA, ED, and MD. (b) Comparison between XENON1T and PandaX-4T based on the VV interaction. The XENON1T limit from Ref. [29] is used for comparison.

总结和展望

1. mass splitting $\delta < O(1\,\mathrm{GeV})$ can still be achieved with the DM mass range considered in this study with the latest PandaX-4T data,

2. several different interactions, including both fermionic and scalar DM are considered. Constraints are provided.

3. Another interesting follow-up study would describe the form factor more precisely